RESEARCH

Actively Tunable Plasmon-Induced Transparency via Alternately Coupled Resonators Based on Bulk Dirac Semimetal Metamaterials

Yong Li[1] · Sa Yang[1] · Qiawu Lin[1] · Shuang Li[1] · Liangpo Tang[1] · Shanna Zhu[1] · Mingyang Su[1]

Abstract

We study the plasmon-induced transparency (PIT) effect in the terahertz domain based on bulk Dirac semimetal (BDS) metamaterials constructed from a cut-wire and a C-shaped resonator pair. With the help of numerical simulations and coupled mode theory, we find that the depth of the transparent window can be adjusted by the coupling distance between the cut-wire and the C-shaped resonator pair. It is further shown that by changing the Fermi level of BDS, the PIT effect can be dynamically tuned without reconstructing the geometry. Simultaneously, the metamaterial structure has excellent sensing properties, which contributes to the theoretical design of bio-chemical sensors. Finally, we further analyze the PIT effect caused by a metamaterial system consisting of a cross-shaped and four C-shaped resonators. Under the illumination of normal incident light along the x- and y-axes in the polarization direction, the device not only produces a PIT effect but also exhibits a strong resonance response consistency for light in both polarization directions, indicating that it exhibits polarization independence for incident terahertz light. This work will provide potential design value for dynamically tunable polarization-independent sensing applications.

Keywords Plasmon-induced transparency · Tunable · Metamaterials · Bulk dirac semimetal

Introduction

The development of optics has always been driven by revolutionary innovative technologies and materials. One of the most typical particles among light manipulators is the metamaterial, which is constructed from artificially tailored metallic or dielectric unit cells. Because metamaterials can be designed to achieve almost any effective electromagnetic parameter value, they have greatly promoted the progress of exotic electromagnetic properties that cannot be achieved by natural materials, including filtering [1, 2], polarization conversion [3, 4], chiral operation [5, 6], sensing [7–10], perfect absorption [11, 12] and nonlinear enhancement [13, 14], etc. In recent years, due to the increasing demand for terahertz (THz) devices, THz technology has made effective progress, and various functional devices based on THz metamaterials for the generation, modulation and detection of THz waves have gradually emerged. It is well known that natural materials have no electromagnetic response in the THz domain, so that metamaterials have become the protagonists of various optical devices designed in the frequency band [15]. Although metamaterials can effectively modulate THz waves, the existence of ohmic and radiation losses can cause the performance of metamaterial devices to be trapped. This dilemma is well resolved thanks to the Fano resonance caused by the destructive interference that occurs between the bright continuum and the dark discrete [16–19].

Among the various Fano resonance effects, the electromagnetically induced transparency (EIT) bred in the three-level atomic system is one of the representatives, which can appear a narrow transparent window in the electromagnetic response spectrum of an opaque object [20]. The conditions required for EIT are extremely harsh, which has led to the construction of its classical analogs, one of which is plasmon-induced transparency (PIT) [21]. PIT based on metamaterials is favored by researchers because of its wide application in switching [22, 23], storage [24, 25], and sensing [26, 27], etc. It has been reported that PIT has been

✉ Yong Li
  leey@hnu.edu.cn

✉ Mingyang Su
  sumy2021@163.com

[1] School of physics and Information Engineering, Guangdong University of Education, Guangzhou 510303, China

produced in various metamaterial structures. *Zhang* et al. first realized the PIT effect in noble metal-based metamaterials by means of bright-dark mode coupling [28]. *Dong* et al. designed PIT by magnetic resonance mode in an asymmetric two-rod configuration [29]. *Miyata* et al. constructed a metallic metamaterial with coupling between dipole and dual-quadrupole to realize the multi-spectral PIT effect [30]. Regrettably, these noble metal-based metamaterial structures are limited by the properties of noble metal materials themselves, which neither support plasmonic responses in the THz domain nor dynamically tune the PIT window.

Since the advent of graphene, it has been widely used in various devices due to its extremely superior electrical and optical properties. Recently, it has been demonstrated both experimentally and theoretically that various rationally designed graphene-based metamaterials can initiate the PIT effect. For example: *Zhao* et al. investigated the PIT effect obtained from a hybrid structure combining a graphene patch and a split-ring resonator [31]. *Sun* et al. proposed a multi-spectral PIT device formed by dielectric-separated bilayer patterned graphene [32]. *Niu* et al. designed T-shaped periodic graphene arrays for active tuning of the PIT effect in the mid-infrared [33]. Although it is remarkable that these graphene-based metamaterial devices can dynamically tune plasmon resonance, the fabrication

process of such ultra-thin two-dimensional (2D) materials is extremely challenging. Now, a novel and peculiar quantum material—bulk Dirac semimetal (BDS), also known as three-dimensional (3D) graphene, has entered the field of vision of researchers [34]. Compared with graphene, BDS not only inherits the dynamic tunability of the conductivity of graphene, but also may have a stronger response to light and be more resistant to environmental defects. In experiments, the conductivity of BDS is usually regulated by altering the Fermi energy (E_F) by means such as alkaline surface doping [35, 36]. Obviously, this novel and easily fabricated bulk material is more suitable for THz metamaterials, which has great implications for the design of tunable devices.

In this paper, a simple in-plane metamaterial structure is proposed to realize the polarization-independent tunable PIT phenomenon, which consists of a cut-wire (CW) and a C-shaped resonator pair. The destructive interference between the CW and the C-shaped resonator pair breeds the PIT effect in this model. We analyze the influence of the coupling distance between the CW and C-shaped resonator pairs on the PIT spectrum. Further investigation found that the transparent window is actively tuned with the change of E_F, which provides a potential design value for dynamically modulating THz waves. In addition, the structure can be found to be sensitive to the refractive index of the surrounding environment, which will provide valuable assistance in sensing applications. Finally, we discuss the response spectrum of a system composed of a cross-shaped and four C-shaped (4 C) resonators under normal incident light whose polarization directions are along the x- and y-axis, respectively. It is clear that the plasmon resonance spectrum exhibits polarization-independent properties for THz light. Therefore, the designed metamaterial structure will provide a potential reference value for applications in modulation and sensing of THz technology.
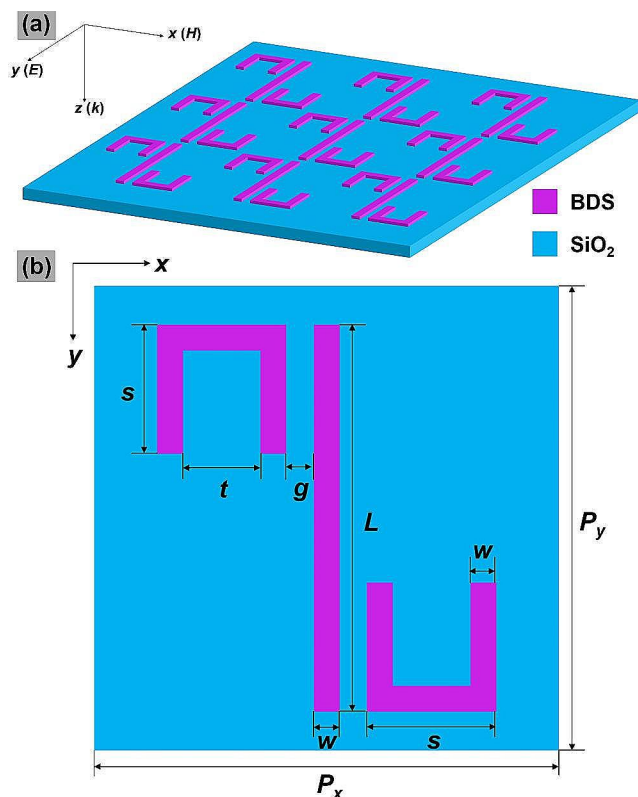
Structure and Theoretical Model

First, a 3D sketch of the designed structure based on the BDS metamaterial is shown in Fig. 1(a), which is an in-plane array consisting of a CW and two C-shaped (2 C) elements resting on a silicon dioxide (SiO_2) substrate. The relevant geometric parameters are depicted in Fig. 1(b). The period of the unit cell of the device is $P_x=P_y=P$, the length, width and thickness of the CW are set to L, w, d, respectively, the size and gap of a single C-shaped element are s and t, respectively, and the coupling distance between CW and 2 C is denoted as g. In the numerical calculation, the specific values of the geometry are taken as $P=100$ μm, $L=70$ μm, $w=g=5$ μm, $s=28$ μm, $t=18$ μm, $d=0.2$ μm.

Fig. 1 (a) The 3D design drawing based on BDS metamaterial; (b) Top view of the structure with associated parameters

In this model, the refractive index of SiO2 is 1.5. The details of the BDS material used in the simulation can be found in Reference [34], and its E_F is set to 210 meV. The values of these related parameters mentioned above are fixed unless otherwise stated.

The transmission spectrum and electromagnetic field distribution of the designed structure are analyzed by means of the 3D finite-difference time-domain (FDTD) method. The y-polarized plane wave propagating along the positive direction of the z-axis hits the BDS-based metamaterial. In order to simulate an infinite simulation domain, periodic boundary conditions are set in the x and y directions, and the perfectly matched layer sandwiching the structure is set in the z direction to absorb reflection and scatter electromagnetic waves to prevent interference.

Results and Discussion

We investigate the transmission spectra of the configurations under normal incidence of THz light with the electric field polarization direction along the y-axis, as shown in Fig. 2(a). The green curve with rhombuses depicts the transmission spectrum where only CW exists, and it is clear that CW supports a strong plasmon resonance at $f = 1.46$ THz. When only the 2 C element exists, the transmission spectrum shows a yellow curve with the ball, and at the same
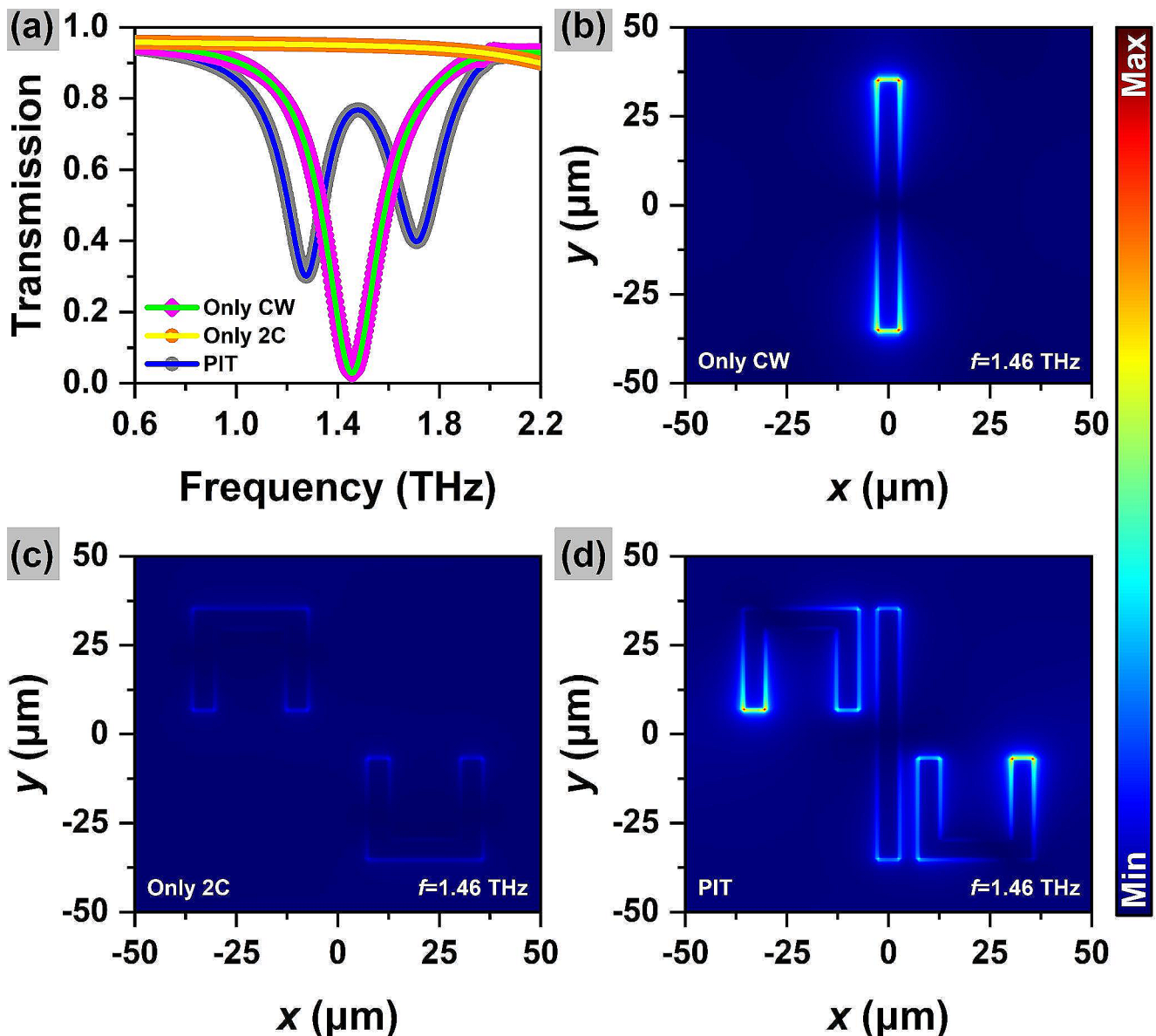

Fig. 2 (a) Transmission spectra for CW, 2 C and PIT under y-polarized THz light. The distribution of the electric field (E) at $f = 1.46$ THz where only CW or 2 C exists is denoted by (b) and (c), respectively. (d) is the electric field (E) distributions at $f = 1.46$ THz in the PIT spectrum

frequency, the 2 C element exhibits LC resonance. Once the CW and 2 C elements are combined, the PIT effect spectrum shown by the blue curve with the ball is formed. In order to clarify the mechanism behind the formation of the PIT effect, the relevant electric field (E) distribution diagram is drawn. Figure 2(b) plots the E distribution where only CW exists. Obviously, CW can directly couple with the incident THz light to cause a dip at $f = 1.46$ THz, so it can be regarded as a bright mode. When only the 2 C element exists in the device, the E at $f = 1.46$ THz is shown in Fig. 2(c). It can be found that the 2 C element can hardly directly couple with the incident THz light, which can be called a dark mode. In this way, the destructive interference between the bright mode and the dark mode gives birth to the PIT effect, which can be proved by the electric field distribution at $f = 1.46$

THz in the PIT curve [28, 37, 38]. As shown in Fig. 2(d), it is obvious that the bright mode is severely suppressed by destructive interference, and only the dark mode is excited through indirect coupling with the bright mode.

Here, the transmission characteristics of the designed BDS-based metamaterial structure are analyzed as the coupling distance g varies. As shown in Fig. 3(a), the red curve with spheres represents the transmission of the structure at $g = 5$ μm. In Fig. 3(b), the magenta line with spheres indicates the transmission at $g = 8$ μm. Whereas in Fig. 3(c) and (d), the orange and purple lines with spheres depict the transmittance of the structure for $g = 11$ μm and $g = 14$ μm, respectively. It can be clearly seen from the green auxiliary line that the frequency point of the transparent peak is almost unchanged with the gradual increase of g, while

Fig. 3 (a), (b), (c) and (d) depict the transmission spectra of the studied structures under $g = 5$ μm, $g = 8$ μm, $g = 11$ μm and $g = 14$ μm, respectively. (e), (f), (g) and (h) show the electric field at the PIT peak of the proposed structure corresponding to (a), (b), (c) and (d), respectively. (i), (j), (k) and (l) are the transmission spectra under coupled mode theory corresponding to (a), (b), (c) and (d), respectively
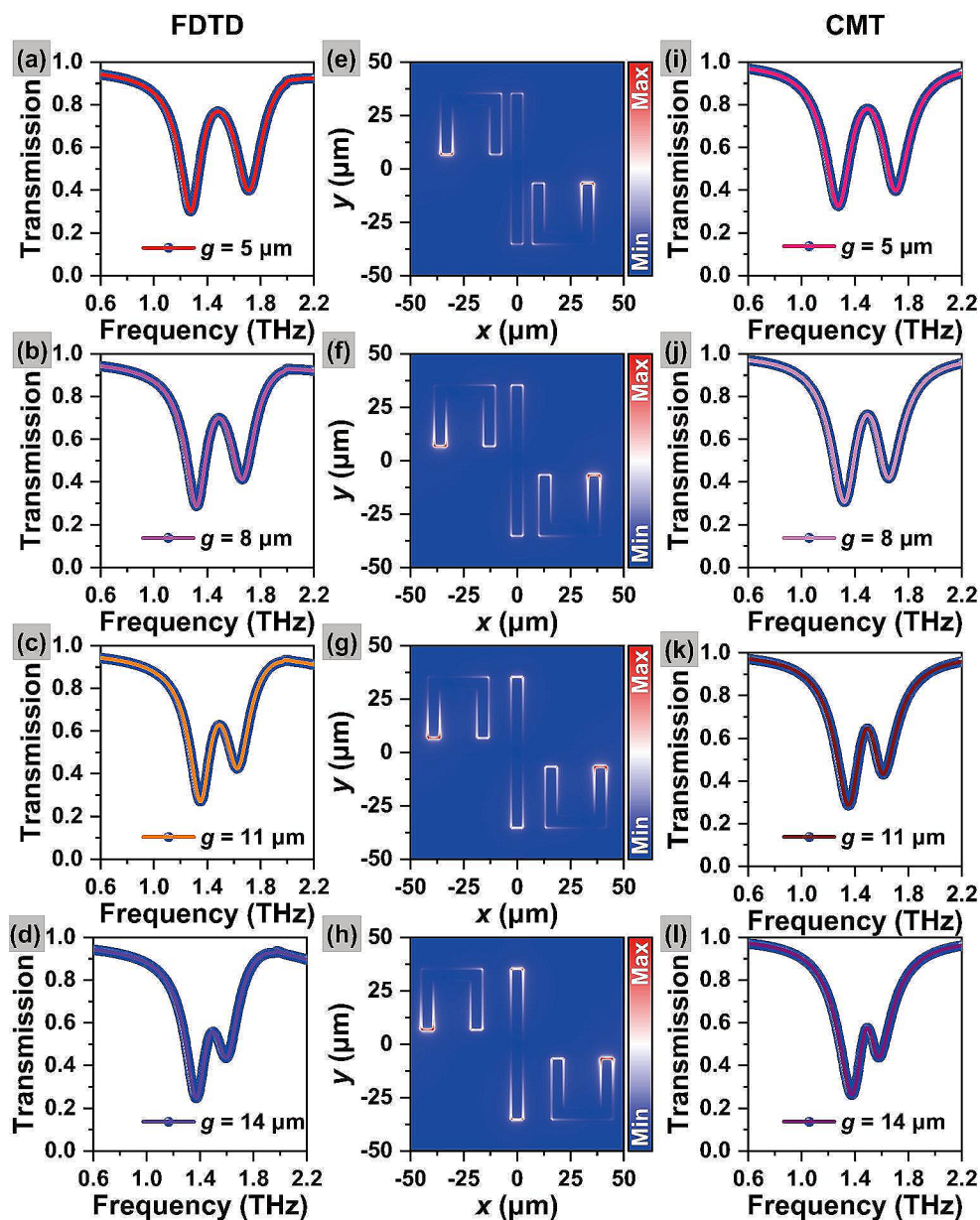
the bandwidth of the transparent window is narrowed and the height is reduced, which is due to the smaller coupling strength between the CW and 2 C components. To further understand the PIT effect based on BDS metamaterials, Fig. 3(e), (f), (g) and (h) show the electric field at the transparent peak under $g = 5$ μm, $g = 8$ μm, $g = 11$ μm and $g = 14$ μm, respectively. It is clear that the device possesses a wider transparent window when the coupling distance between the CW and 2 C elements is $g = 5$ μm (see Fig. 3(a)). Once the 2 C elements gradually move away from the CW, the coupling strength between them becomes smaller. When $g = 14$ μm, the CW and 2 C elements are almost decoupled, which makes the PIT effect of the system weaken and the transparent window narrow. In this way, we know that the above-mentioned changing behavior of the spectrum can better tune the PIT effect by changing the coupling strength between CW and 2 C elements.

In order to clarify the mechanism of PIT, a three-level atomic system model can be introduced. There are two states in the three-level atomic system model, namely, a strongly coupled mode (bright mode) directly coupled by incident light and a weakly coupled mode (dark mode). Therefore, the destructive interference between the paths |0>-|1> and |0>-|1>-|2>-|1> creates the PIT effect. |0>-|1> is the path from the ground state (incident field) to the excited state. |0>-|2> are paths that cannot be directly implemented. However, |2> can be excited by coupling through |1>-|2>. With the help of coupled mode theory (CMT), the field amplitudes of the two states can be described as [39, 40]:

$$(\omega - \omega_1 + i\gamma_1)a_1 + \kappa a_2 = -\eta E$$
$$(\omega - \omega_2 + i\gamma_2)a_2 + \kappa a_1 = 0 \qquad (1)$$

Here, ω_1, ω_2 and γ_1, γ_2 are the resonant frequency and damping factor of the two modes (bright mode and dark mode), respectively. ω is the frequency of the incident light, κ and η are the coupling coefficients between the bright and dark modes and the parameters of the coupling strength between the bright mode and the incident electromagnetic field (E), respectively. The solution to Eq. (1) can be written as:

$$a_1 = \frac{\eta E(\omega - \omega_2 + i\gamma_2)}{\kappa^2 - (\omega - \omega_1 + i\gamma_1)(\omega - \omega_2 + i\gamma_2)} \qquad (2)$$

Therefore, with the help of the formula $t(\omega) = 1 - |a_1/E|^2$, the transmittance of the system is obtained [39]:

Table 1 Fitting parameters under different coupling distances g

g (μm)	η (THz)	γ_1 (THz)	γ_2 (THz)	κ (THz)
5	0.1494	0.0595	0.1787	0.2151
8	0.1482	0.0980	0.1334	0.1543
11	0.1473	0.1233	0.1020	0.1118
14	0.1459	0.1396	0.0777	0.0795

$$t(\omega) = 1 - \left| \frac{\eta(\omega - \omega_2 + i\gamma_2)}{\kappa^2 - (\omega - \omega_1 + i\gamma_1)(\omega - \omega_2 + i\gamma_2)} \right|^2 \qquad (3)$$

Under the analysis of CMT, the transmittance of the system is shown in Fig. 3(i)-(l). It is obvious that CMT proves the correctness of numerical calculations very well. In order to clarify the influence of physical quantities on the resonance spectrum, the fitting parameters of different coupling distances g under the CMT are shown in Table 1. Clearly, as the coupling distance g increases, the coupling parameter κ decreases. Due to the reduction in coupling strength, the excitation of the dark mode is weakened, and the electric field suppression of the CW is not significant, which means that the electromagnetic energy of the CW is enhanced. Therefore, the damping rate γ_1 in the bright mode increases. However, the damping rate γ_2 decreases in dark mode.

Next, we explore the proposed structure to form the PIT effect with active tunability by changing the E_F of the BDS material. Figure 4(a) depicts the contour map of the transmission based on the BDS metamaterial structure at different E_F values. Initially, $E_F = 140$ meV, and the frequency of the transparent peak is at $f = 1.39$ THz. In the process of gradually increasing E_F to 220 meV, the resonance frequency of the transparent peak also increases accordingly, and finally reaches $f = 1.49$ THz. From Fig. 4(a), it can be found that as the E_F increases, the transparent window shows a blue-shift, and its transmittance becomes larger. Evidently, the resonant frequency at the transparent peak has a strong dependence on E_F. Here, 2 C can be regarded as a small inductive-capacitive (LC) circuit. Inductance (L) and capacitance (C) can effectively tune the resonant frequency. The connection between them can be written as:

$$f \propto \frac{1}{\sqrt{LC}} \propto \frac{1}{\sqrt{(L_g + L_k)C}} \qquad (4)$$

Among them, the geometric inductance L_g and the kinetic inductance L_k are controlled by the geometric parameters and $m_e/(n_e e^2)$, respectively. e, m_e, and n_e are the electron charge, electron mass, and carrier concentration respectively [41]. As long as the Fermi level increases, the conductivity will increase, resulting in an increase in carrier concentration, causing L_k to decrease, and the PIT spectrum will undergo a blue-shift. Therefore, varying the E_F of the BDS material can lead to efficient tuning of the PIT spectrum of the designed structure without reconfiguring the geometry. This may provide potential design ideas for dynamic modulation devices based on BDS metamaterials. Moreover, we further simulated the response feature of the structure to the refractive index (n) of the surrounding environment. In Fig. 4(b), adjusting the n from 1.0 to 1.4, the transparency peak moves from $f = 1.48$ THz to $f = 1.30$ THz.

Fig. 4 (a) Contour plot of the transmission spectrum of the structure with tuning of the E_F of the BDS material. (b) Contour plot of the PIT spectra for different n
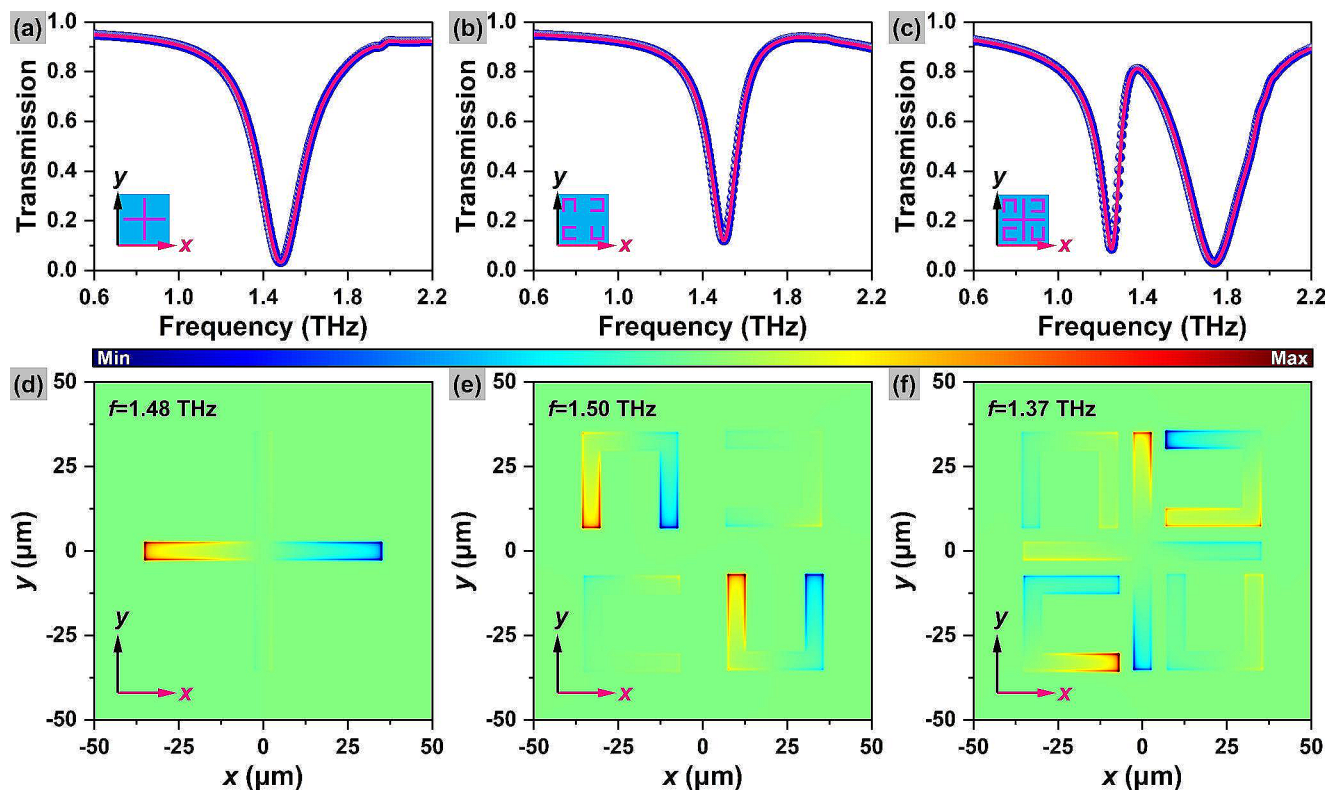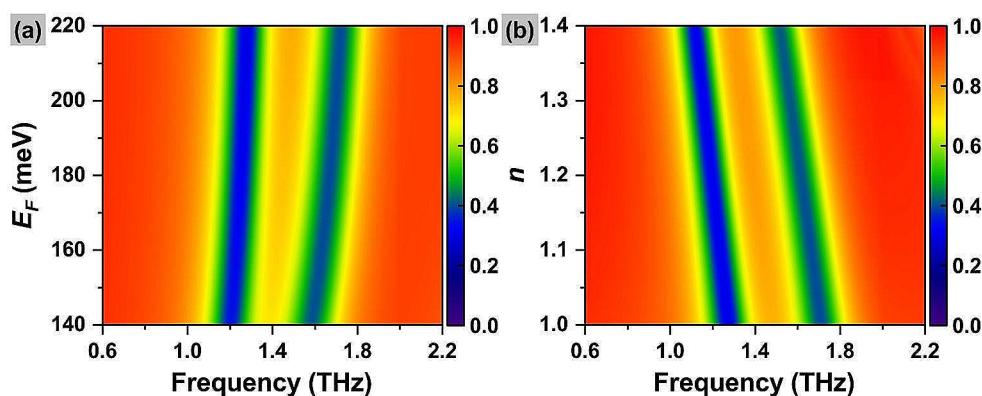

Fig. 5 Transmission spectra of (a) cross-shaped element, (b) 4 C element, and (c) PIT effect under x-polarized THz light. Electric field distributions of (d) cross-shaped element, (e) 4 C element, and (f) PIT window at $f=1.48$ THz, $f=1.50$ THz, and $f=1.37$ THz, respectively. Pink arrow indicates the polarization direction of THz light

When n increases, the transmittance of the transparent window remains almost constant, and the two dips of the PIT spectrum undergo obvious red shifts. Obviously, the PIT effect is more sensitive to the surrounding refractive index, so the sensitivity can be defined as [42]:

$$SS = \frac{\Delta\lambda}{\Delta n} \qquad (5)$$

Here $\Delta\lambda$ and Δn are the amounts of spectral shift and refractive index change, respectively. The calculation results show that the wavelength increment corresponding to the unit refractive index change is $SS = 110$ μm/RIU, here Δn is chosen to be 0.01. To better quantify the figure of merit (FOM), the FOM can be written [43]:

$$FOM = \frac{SS}{FWHM} \qquad (6)$$

where FWHM is the full width at half maximum of the spectrum. Choosing Δn to be 0.01, the obtained FOM is approximately 2 at 203 μm ($f=1.48$ THz). Consequently, it can be found that the structure is sensitive to the n of the surrounding environment, which is extremely important and

can provide a potential platform for the application of THz plasmonic sensing devices.

From the structure based on the BDS metamaterial studied above, it can be found that the condition for the effective generation of the PIT effect is that the polarization direction of the incident THz light is parallel to the CW. This feature has strong limitations in some composite application scenarios, and it is urgent to develop polarization-independent PIT responses. To this end, CW and 2 C elements are additionally added in the vertical direction of the structure proposed above to obtain the polarization-independent PIT phenomenon. Figures 5 and 6 depict the transmission and electric field distributions of the new metamaterial system constructed from a cross-shaped element and 4 C elements under polarization along the x and y axes, respectively. In Figs. 5 and 6, the pink arrow illustrates the polarization direction of THz light, and the red curves with spheres and cyan curves with spheres represent the transmission spectra of the new system under x-polarization and y-polarization, respectively. The polarization-independent PIT effect is easily elucidated by the transmission spectra in Figs. 5 and 6 combined with the corresponding electric field distribution. It is clear that the electromagnetic response of the new system to two polarized THz light is highly consistent. When only the cross-shaped element is present, the transmission

for x-polarization and y-polarization is shown in Fig. 5(a) and 6(a), respectively. However, when only 4 C elements are present, the transmission of x-polarization and y-polarization are shown in Fig. 5(b) and 6(b), respectively. The cross-shaped element supports a strong plasmonic response at $f = 1.48$ THz, while the 4 C element exhibits an LC resonance at $f = 1.50$ THz. In Fig. 5 (a) and (b), the FWHM of the transmission spectrum is calculated to be $\Delta\lambda = 37.2$ μm and 22.4 μm, respectively. Define $Q = \lambda_0/\Delta\lambda$, and λ_0 is the response wavelength at the PIT window. Then the Q factors of the cross-shaped element and the 4 C element are approximately 5.4 and 8.9, respectively. From Fig. 5(a) and (b) or Fig. 6(a) and (b), it can be found that the 4 C element has a narrower and shallower transmission than the cross-shaped element. In this case, the response supported by the cross-shaped element can be referred to as bright mode and the resonance exhibited by the 4 C element as dark mode. Once there is coupling between the two response modes, a clear transparent peak appears, which originates from the destructive interference between the two modes. Figure 5(c) and Fig. 6(c) plot the PIT spectra for x-polarization and y-polarization, respectively. It can be proved that the response of the designed new structure to THz light is polarization-independent, which is due to the fact that the PIT effect caused by the two kinds of polarized light is equally strong.
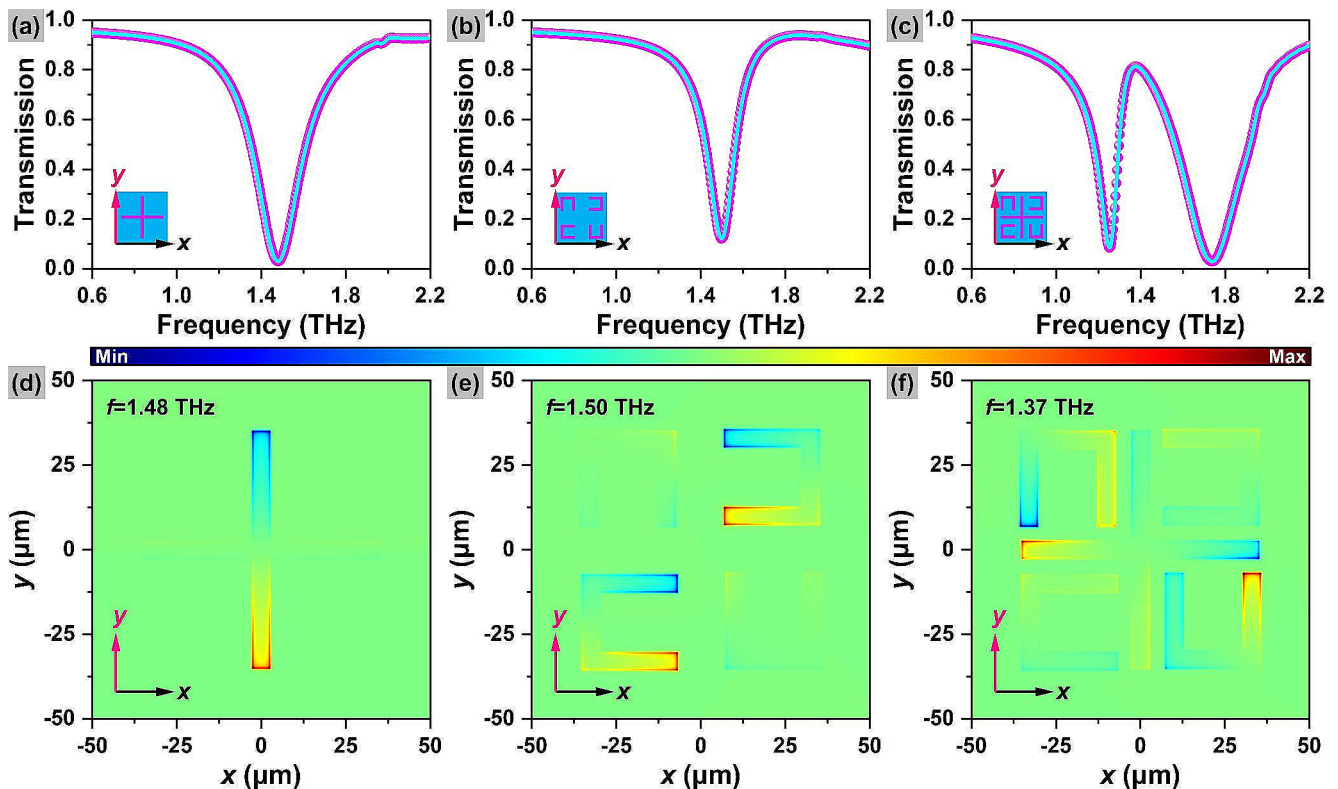

Fig. 6 Transmittance of (a) cross-shaped element, (b) 4 C element, and (c) PIT effect under y-polarized THz light. Electric field distributions of (d) cross-shaped element, (e) 4 C element, and (f) PIT peak at $f = 1.48$ THz, $f = 1.50$ THz, and $f = 1.37$ THz, respectively. The polarization of THz light is parallel to the pink arrow direction

Fig. 7 (a) and (b) show the transmission spectra under *x*-polarization and *y*-polarization at different Fermi levels, respectively. (c) and (d) illustrate the contour plots of the transmission spectrum of incident THz light under *x*-polarization and *y*-polarization, respectively. Pink arrow depicts the polarization direction of the incident electric field
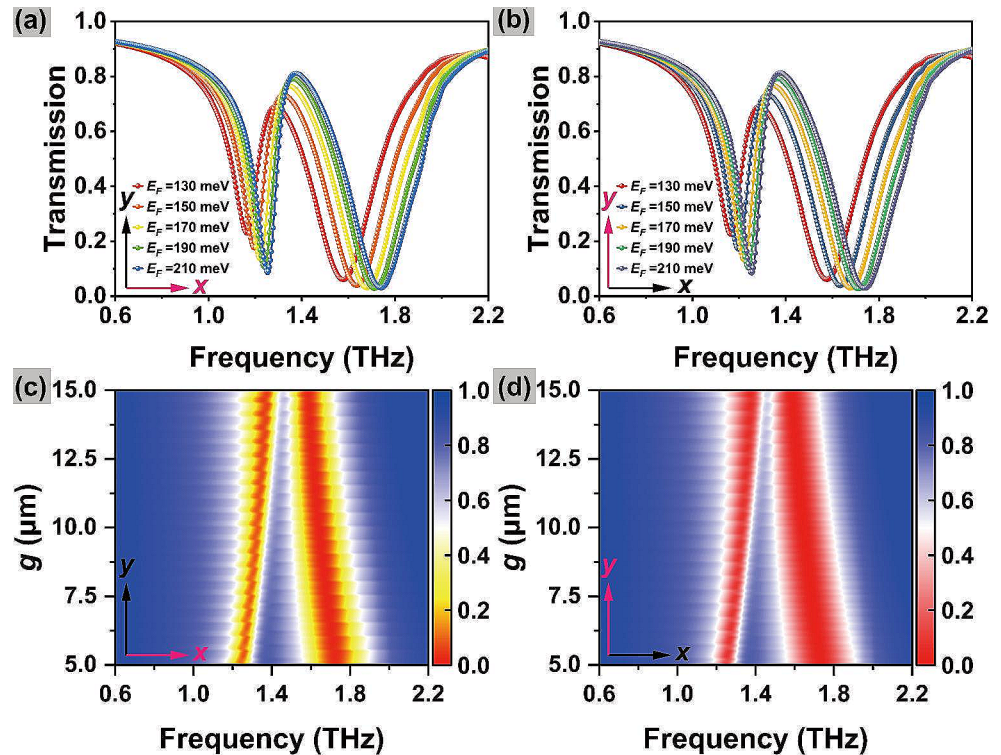
At the same time, the electric field distributions of the cross-shaped element, 4 C element and the new metamaterial structure under *x*-polarization and *y*-polarization are given in Figs. 5 and 6, respectively. The polarization of the incident THz light is parallel to the magenta arrow direction. Figure 5(d) and Fig. 6(d) depict the *x*-polarized and *y*-polarized electric fields at $f = 1.48$ THz in the presence of only the cross-shaped element, respectively. However, the *x*-polarized and *y*-polarized electric fields at $f = 1.50$ THz in the presence of only 4 C elements are illustrated in Fig. 5(d) and Fig. 6(d), respectively. It can be noticed that, regardless of *x*-polarization or *y*-polarization, only the CW elements parallel to the polarization of the incident THz light in the cross-shaped structure can be excited. Whereas, in the 4 C structure, the C-shaped element whose opening direction of the gap is parallel to the polarization cannot be lit. When these modes are supported to couple with each other, a significant PIT window results from the destructive interference between the modes. Under *x*-polarization and *y*-polarization, the electric field distribution at the transparent peak, that is, $f = 1.37$ THz, is shown in Fig. 5(f) and 6(f), respectively. It is obvious that the CW element parallel to the polarization is almost suppressed, exactly caused by destructive interference.

Finally, we further discuss the properties of the newly designed BDS-based metamaterial system for tuning the transparent window. As shown in Fig. 7, the transmission spectrum of the system constructed from the cross-shaped element and the 4 C elements. As the Fermi level of the BDS

material gradually increases, the transmission spectra along the *x*-polarization and *y*-polarization are significantly blue-shifted, as shown in Fig. 7(a) and (b), respectively. It can be seen from Eq. 4 that due to the increase in Fermi level, the conductivity increases, further promoting the increase in carrier concentration, resulting in a decrease in L_k. Increasing the value of the coupling distance *g* causes the C-shaped element to move away from the cross-shaped element. Therefore, under the *x*-polarization and *y*-polarization of the incident THz light, as the *g* value changes, the characteristics of the PIT transmission spectrum are shown in Fig. 7. Figure 7(c) illustrates a contour plot of the transmission of incident THz light for *x*-polarization, while Fig. 7(d) shows a contour plot of the transmission spectrum of incident THz light for *y*-polarization. It can be clearly seen that the severity of the PIT response of the new system is consistent for *x*-polarization or *y*-polarization. Meanwhile, we can understand that the bandwidth of the PIT spectrum is narrowing and the height of the transparent peak is gradually decreasing as *g* increases from 5 to 15 μm. These features above indicate that it is very practical to design polarization-independent modulation devices in the THz domain.

Conclusions

In conclusion, we numerically and theoretically investigate a BDS-based metamaterial composed of CW and 2 C elements. The PIT effect conceived by the proposed device

originates from the destructive interference of the CW element and the 2 C element in response to THz light. At the same time, increasing the coupling distance between CW and 2 C elements, although the resonant frequency of the transparent window is almost unchanged, its bandwidth is narrowed, and the height of the transparent peak becomes lower. In addition, we explored that increasing the E_F of BDS materials can promote the blue-shift of the transparent window. Furthermore, this configuration was found to be sensitive to the surrounding ambient refractive index and could be used as bio-chemical sensing. Finally, we further propose that the BDS-based structure constructed by the cross-shaped element and the 4 C element realizes the polarization-independent PIT response. Once the 4 C element is gradually moved away from the CW element, the transparent window will be narrowed due to weaker coupling strength. The investigated structure may provide design solutions for the development of potential THz functional devices such as sensing, modulation and switching.

Declarations

References

1. Yang W, Lin Y-S (2020) Tunable metamaterial filter for optical communication in the terahertz frequency range. Opt Express 28:17620–17629

2. Pitchappa P, Kumar A, Singh R, Wang N (2022) Electromechanically tunable frequency-agile Metamaterial Bandpass filters for Terahertz waves. Adv Opt Mater 10:2101544

3. Zi J, Xu Q, Wang Q, Tian C, Li Y, Zhang X, Han J, Zhang W (2018) Antireflection-assisted all-dielectric terahertz metamaterial polarization converter. Appl Phys Lett 113:101104

4. Jing X, Gui X, Zhou P, Hong Z (2018) Physical explanation of Fabry–Pérot cavity for Broadband Bilayer metamaterials polarization converter. J Lightwave Technol 36:2322–2327

5. Kindness SJ, Almond NW, Michailow W, Wei B, Delfanazari K, Braeuninger-Weimer P, Hofmann S, Beere HE, Ritchie DA (2020) Degl'Innocenti, a Terahertz Chiral Metamaterial Modulator. Adv Opt Mater 8:2000581

6. Bai J, Yao Y (2021) Highly efficient Anisotropic Chiral Plasmonic metamaterials for Polarization Conversion and Detection. ACS Nano 15:14263–14274

7. Yang J, Lin Y-S (2021) Design of Tunable Terahertz Metamaterial Sensor with single- and Dual-Resonance Characteristic. in: Nanomaterials,

8. Hua Y, Tang W, Cui TJ (2022) A metamaterial sensor for detecting the location of a sub-wavelength object. Appl Phys Lett 120:181703

9. Islam M, Kumar Bhowmik B, Dhriti KM, Minakshi D, Mohan A, Ahmad G, Kumar (2022) Thin film sensing in a planar terahertz meta-waveguide. J Opt 24:064016

10. Islam M, Rao SJM, Kumar G, Pal BP (2017) Roy Chowdhury, Role of Resonance modes on Terahertz metamaterials based Thin Film Sensors. Sci Rep 7:7355

11. Landy NI, Sajuyigbe S, Mock JJ, Smith DR, Padilla WJ, Absorber PM (2008) Phys Rev Lett 100:207402

12. Loh JYY, Safari M, Mao C, Viasus CJ, Eleftheriades GV, Ozin GA, Kherani NP (2021) Near-Perfect Absorbing Copper Metamaterial for Solar Fuel Generation. Nano Lett 21:9124–9130

13. Suresh S, Reshef O, Alam MZ, Upham J, Karimi M, Boyd RW (2021) Enhanced nonlinear optical responses of layered Epsilon-near-zero metamaterials at visible frequencies. ACS Photonics 8:125–129

14. Wang Y, Lang L-J, Lee CH, Zhang B, Chong YD (2019) Topologically enhanced harmonic generation in a nonlinear transmission line metamaterial. Nat Commun 10:1102

15. Zheludev NI (2010) The Road ahead for metamaterials. Science 328:582–583

16. Wu C, Khanikaev AB, Shvets G (2011) Broadband slow light Metamaterial based on a double-Continuum Fano Resonance. Phys Rev Lett 106:107403

17. Gupta M, Singh R (2016) Toroidal versus Fano resonances in High Q planar THz metamaterials. Adv Opt Mater 4:2119–2125

18. Sarkar R, Ghindani D, Devi KM, Prabhu SS, Ahmad A, Kumar G (2019) Independently tunable electromagnetically induced transparency effect and dispersion in a multi-band terahertz metamaterial. Sci Rep 9:18068

19. Bhattacharya A, Sarkar R, Sharma NK, Bhowmik BK, Ahmad A, Kumar G (2021) Multiband transparency effect induced by toroidal excitation in a strongly coupled planar terahertz metamaterial. Sci Rep 11:19186

20. Islam M, Dhriti KM, Sarkar R, Kumar G (2021) Tunable control of electromagnetically induced transparency effect in a double slot terahertz waveguide. Opt Commun 483:126632

21. Dhriti KM, Islam M, Bhattacharya A, Ahmad A, Kumar G (2021) Plasmon-induced transparency in an air–dielectric grooved parallel-plate terahertz waveguide. J Opt Soc Am B 38:1290–1296

22. Zhang X, Liu Z, Zhang Z, Gao E, Luo X, Zhou F, Li H, Yi Z (2020) Polarization-sensitive triple plasmon-induced transparency with synchronous and asynchronous switching based on monolayer graphene metamaterials. Opt Express 28:36771–36783

23. Ling Y, Huang L, Hong W, Liu T, Luan J, Liu W, Lai J, Li H (2018) Polarization-controlled dynamically switchable plasmon-induced transparency in plasmonic metamaterial. Nanoscale 10:19517–19523

24. Bai Z, Xu D, Huang G (2017) Storage and retrieval of electromagnetic waves with orbital angular momentum via plasmon-induced transparency. Opt Express 25:785–798

25. Gao E, Li H, Liu Z, Xiong C, Liu C, Ruan B, Li M, Zhang B (2020) Terahertz multifunction switch and optical storage based on triple plasmon-induced transparency on a single-layer patterned graphene metasurface. Opt Express 28:40013–40023

26. Tang P-r, Li J, Du L-h, Liu Q, Peng Q-x, Zhao J-h, Zhu B, Li Z-r (2018) -g. Zhu, Ultrasensitive specific terahertz sensor based on tunable plasmon induced transparency of a graphene micro-ribbon array structure. Opt Express 26:30655–30666

27. He Z, Cui W, Ren X, Li C, Li Z, Xue W, Zhang B, Zhao R (2020) Ultra-high sensitivity sensing based on tunable plasmon-induced transparency in graphene metamaterials in terahertz. Opt Mater 108:110221

28. Zhang S, Genov DA, Wang Y, Liu M, Zhang X (2008) Plasmon-Induced transparency in metamaterials. Phys Rev Lett 101:047401

29. Dong Z-G, Liu H, Xu M-X, Li T, Wang S-M, Zhu S-N, Zhang X (2010) Plasmonically induced transparent magnetic resonance in a metallic metamaterial composed of asymmetric double bars. Opt Express 18:18229–18234

30. Miyata M, Hirohata J, Nagasaki Y, Takahara J (2014) Multi-spectral plasmon induced transparency via in-plane dipole and dual-quadrupole coupling. Opt Express 22:11399–11406

31. Zhao X, Yuan C, Lv W, Xu S, Yao J (2015) Plasmon-Induced transparency in Metamaterial based on Graphene and Split-Ring resonators. IEEE Photon Technol Lett 27:1321–1324

32. Sun C, Si J, Dong Z, Deng X (2016) Tunable multispectral plasmon induced transparency based on graphene metamaterials. Opt Express 24:11466–11474

33. Niu Y, Wang J, Hu Z, Zhang F (2018) Tunable plasmon-induced transparency with graphene-based T-shaped array metasurfaces. Opt Commun 416:77–83

34. Kotov OV, Lozovik YE (2016) Dielectric response and novel electromagnetic modes in three-dimensional Dirac semimetal films. Phys Rev B 93:235417

35. Liu ZK, Jiang J, Zhou B, Wang ZJ, Zhang Y, Weng HM, Prabhakaran D, Mo SK, Peng H, Dudin P, Kim T, Hoesch M, Fang Z, Dai X, Shen ZX, Feng DL, Hussain Z, Chen YL (2014) A stable three-dimensional topological Dirac semimetal Cd3As2. Nat Mater 13:677–681

36. Parameswaran SA, Grover T, Abanin DA, Pesin DA, Vishwanath A (2014) Probing the Chiral Anomaly with Nonlocal Transport in three-Dimensional Topological Semimetals. Phys Rev X 4:031035

37. Devi KM, Sarma AK, Chowdhury DR, Kumar G (2017) Plasmon induced transparency effect through alternately coupled resonators in terahertz metamaterial. Opt Express 25:10484–10493

38. Devi KM, Islam M, Chowdhury DR, Sarma AK, Kumar G (2017) Plasmon-induced transparency in graphene-based terahertz metamaterials. EPL 120:27005

39. Cheng H, Chen S, Yu P, Duan X, Xie B, Tian J (2013) Dynamically tunable plasmonically induced transparency in periodically patterned graphene nanostrips. Appl Phys Lett 103:203112

40. Sarkar R, Devi KM, Ghindani D, Prabhu SS, Chowdhury DR, Kumar G (2020) Polarization independent double-band electromagnetically induced transparency effect in terahertz metamaterials. J Opt 22:035105

41. Linden S, Enkrich C, Dolling G, Klein, MW, Zhou, J, Koschny, T, Soukoulis, CM, Burger, S, Schmidt, F, Wegener, M (2006) Photonic metamaterials: Magnetism at Optical frequencies. IEEE J Sel Top Quantum Electron 12:1097–1105

42. Dolatabady A, Asgari S, Granpayeh N (2018) Tunable mid-infrared Nanoscale Graphene-based refractive Index Sensor. IEEE Sens J 18:569–574

43. Sherry LJ, Chang S-H, Schatz GC, Van Duyne RP, Wiley BJ, Xia Y (2005) Localized Surface Plasmon Resonance Spectroscopy of single silver nanocubes. Nano Lett 5:2034–2038